The effect of slip casting parameters on the ultrafine microstructure and density of pore-free YAG ceramic obtained by vacuum sintering

G. Kafili[1], B. Movahedi*,[1], M. Milani[2]

[1]*Department of Nanotechnology Engineering, Faculty of Advanced Sciences and Technologies, University of Isfahan, Isfahan, Iran.*

[2]*Department of Advanced Materials and Renewable Energies, Iranian Research Organization for Science and Technology, Tehran, Iran.*

ABSTRACT

In this study, the effect of slip casting parameters on the ultrafine microstructure and the density of pore-free YAG ceramic was evaluated. A stable, high concentrated aqueous YAG slurry using Dolapix-CE64 as a dispersant was prepared and the effect of dispersant concentration as well as the solid load on the stability and rheological behavior of the slurry was also studied. The optimum dispersant content for the suspension was 1.5 wt% which led to the slurry with minimum viscosity and near-Newtonian behavior. The results showed that increasing the solid load of the YAG slurry causes higher viscosity and alters the rheological behavior of the slurry to a slight shear thinning. By increasing the solid load of the slurry up to a specific amount of 75 wt%, relative green density of the slip cast sample was increased to about 65%, but further increase reduced the green density. The microstructure and the density of the sintered body in the air and vacuum atmospheres comprise a direct relationship to the green density of the slip cast body.

Key words: YAG, slip casting, rheological behavior, ultrafine microstructure, sintering.

1. Introduction

Yttrium aluminum garnet (YAG, $Y_3Al_5O_{12}$) is an advanced oxide ceramic with outstanding structural and functional properties such as excellent high-temperature strength, low creep rate, and good mechanical and optical properties [1]. YAG ceramic is suitable for laser gain host crystal and IR transparent window material [2]. Low pore concentration, clean grain boundaries, and also phase purity are essential factors in manufacturing transparent ceramics [3, 4]. Among these factors, both the number and the size of the pores are the most important factors which affect the optical properties of transparent ceramics due to the scattering loss caused by the interface between the air in the pores and the ceramic matrix [5]. Therefore, the high-purity precursor as well as processing and forming methods are needed. Previous studies on YAG forming methods were typically focused on slip casting [5-15], dry pressing [16-21], and Isostatic pressing [20, 22-25]. It has been proved that in dry pressing method, the external force cannot reach to an individual particle of the body in order to shift it into an optimum position between its neighbors. However, in colloidal forming processes such as slip casting

and gel casting, the necessary freedom for particles to find an appropriate position on their own can be provided [26]. Slip casting is an effective process in producing homogeneous and dense green bodies because defects such as aggregates and agglomerates can be more readily managed [9, 27].

In most of the reported researches about the slip casting of YAG ceramic, a mixture of Al_2O_3 and Y_2O_3 powders with different dispersant agents such as poly acrylic acid (PAA) [7], Dolapix PC21 and PC75 [11], Dolapix CE64 [10, 14, 15], ammonium poly acrylic acid (NH_4PAA) [5, 8], and Dispex A [9] is ball milled in an aqueous medium to obtain a homogeneous suspension for the slip casting. In these literatures, phase formation of pure YAG occurs during the sintering process at high temperatures. Lv et al. [12] and Li et al. [6] have reported the dependence of rheological properties of co-precipitated powder slurries on pH, solid loading, and the concentration of dispersant agent for YAG and Nd:YAG, respectively. They have ball milled the co-precipitated YAG powder with ammonium poly acrylate as a dispersant agent.

A key point for obtaining homogeneous and dense green bodies with uniform pore size distribution by the slip casting method is achieving a well-dispersed slurry with an appropriate rheological behavior, low viscosity, and relatively high solid loading [28, 29]. The properties of slurries can be adjusted by the shape of particles, fraction of solid particles, dispersant agent concentration, and pH of the slurry. Also, the size of the particles is another important factor for obtaining well-dispersed suspensions. In the case of using nanoparticles, higher agglomeration forces deteriorate the homogeneity of green bodies as well as the sintering densification. It has been reported by Krell et al. [30] that by using nano powders, it is difficult to reach high densities (>99%). Furthermore, the low surface area of particles larger than 300-500 nm used in the slip casting method may not cause successful densification [31]. It is proved that particle size in the range of 100-300 nm is proper for obtaining dense slip cast green bodies with an appropriate sintering behavior [30-32].

Until now, spark plasma sintering, hot pressing, and vacuum sintering have been adopted for fabricating transparent and dense ceramics. However, transparency is not a necessary property for engineering applications and pressureless sintering in the air can be considered as a cost-effective method for developing dense ceramics

[33]. Bhattacharyya et al. [34] have reported pressureless sintering of YAG ceramic in the presence of 2.5% fumed silica additive, achieving 93% relative density. Dense YAG ceramics sintered in the air using TEOS and MgO as a sintering aid have been developed by Tong et al. [33].

Many researchers have studied the effective parameters on the slip casting of Al_2O_3 and Y_2O_3 mixture and co-precipitated YAG powders. However, the effect of solid loading and dispersant concentration on the rheological behavior of YAG slurries derived from Al_2O_3/Y-compound core-shell structures [35-40] have not been evaluated yet. Therefore, in the present study, the effects of various slip casting parameters such as dispersant concentration and solid loading on the rheological behavior of core-shell derived YAG slurries as well as the green density of slip cast bodies were investigated. Finding the best dispersion parameters for obtaining stable suspensions of YAG with high solid loading and preferably Newtonian behavior was the most important goal of this study. In this approach, we also reported the fabrication of ultrafine YAG ceramics with high densities, sintered in the air and vacuum atmospheres without using any sintering aid. Pre-forming of YAG green bodies with high densities helps to reach a dense YAG ceramic even without using any sintering aid. The green and sintered bodies were thoroughly characterized in terms of microstructure and density.

2. Experimental procedures

The ultrafine YAG powders were synthesized via a partial wet route, details of which are reported elsewhere [37, 38]. The calcined YAG powders were de-agglomerated in a planetary ball mill for 15h using 10 mm alumina balls. In this study, Dolapix CE64 (Zschimmer & Schwarz Chemical Co., Ltd.) was chosen as a dispersant agent with concentrations varying from 0.5 to 2.5 wt% for preparing the YAG slurries. Slurries of the de-agglomerated ultrafine YAG powders prepared by dispersing to different solid loadings (55-80 wt%) in deionized water with 1.5 wt% Dolapix dispersant were cast on an alumina template to obtain green bodies. Hand-made alumina templates were slip casted and then sintered at oxygen atmosphere. The relative density of a template after sintering is about 70%. After slip casting of YAG slurries on the alumina template, the bodies were dried in the air and the organic additives were removed

by heating the samples at 600°C for 2h. Then, slip casted samples were sintered in both air and vacuum atmospheres. Under the air atmosphere, the sintering temperature and the soaking time were 1720°C and 12h, respectively. At the vacuum sintering, the specimens were heated up to 1700°C and held for 12h. The rate of heating for both sintering methods was chosen as 10°C/min. The sintered bodies were annealed at 1250°C for 3h in the air in order to remove the gray color. Relative green density and relative density after sintering were measured using the Archimedes method (ASTM B962-13) [41], assuming a theoretical density of YAG is 4.5488 g/cm³ [6].

Rheological properties of the slurries were determined up to a shear rate of 264 s⁻¹ with a rotational stress-controlled viscometer (Model LVDV-II; Brookfield, Middleboro, USA). All measurements were performed at a constant temperature (25°C). Microstructural evaluation of green and sintered bodies as well as the morphology of powders was observed using field emission scanning electron microscopy (FESEM, Tescan Mira III). The particle size distribution of

the synthesized and de-agglomerated powders was measured using dynamic light scattering (DLS, Vasco, Oakbrook Terrace. IL, USA). X-ray diffraction (XRD) pattern was recorded on the Bruker D8 Advance X-ray diffractometer with Cu Kα (λ= 0.15406 nm). Pore size distribution of the slip cast green body was measured using Mercury porosimetry (PoreSizer 9320, Micromeritics Instrument Corporation, USA).

3. Results and discussion

Fig. 1 shows the XRD pattern of synthesized ultrafine powder calcined at 1400°C for 3h. All peaks can be identified as $Y_3Al_5O_{12}$ (abbreviated as YAG, JCPDS card No. 33-0040) phase. The micrographs of synthesized and de-agglomerated YAG powder are shown in Fig. 2. Particles with necking phenomenon can be observed in Fig. 2(a). The mean particle size of the synthesized ultrafine YAG powder is about 500-600 nm. Uniform separate particles with a diameter of about 250-300 nm are obtained after the de-agglomeration process (Fig. 2(b)).

Fig. 3 illustrates the particle size distribution
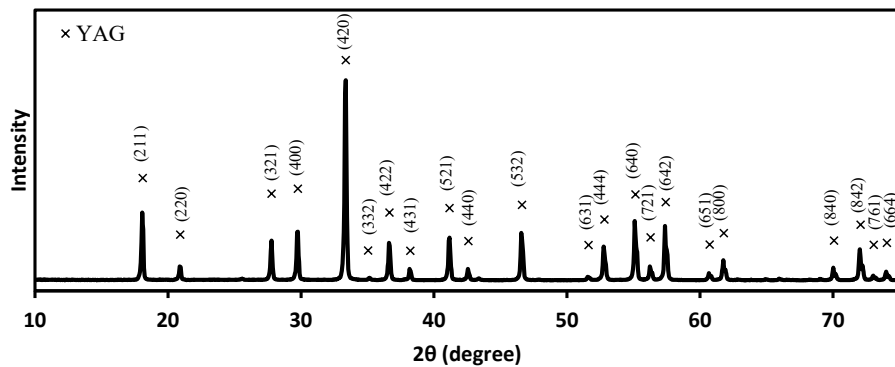
Fig. 1- XRD pattern of the synthesized powder calcined at 1400°C for 3h.
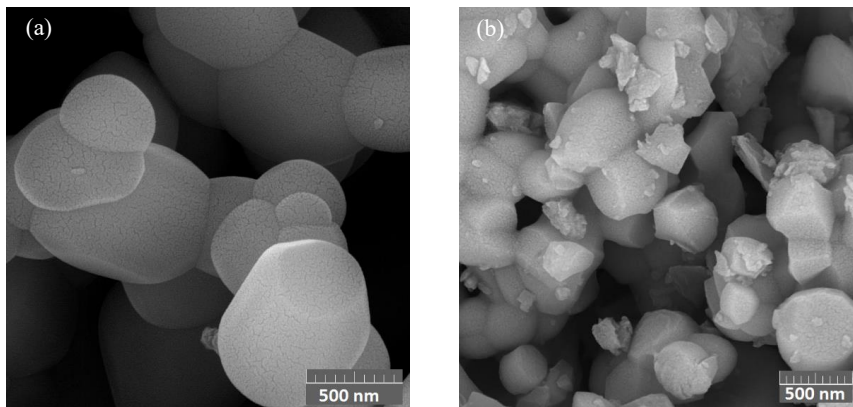
Fig. 2- FESEM images of (a) YAG powder, (b) de-agglomerated ultrafine YAG powder.

of synthesized and de-agglomerated ultrafine YAG powders. There are two peaks located at 568 and 1725 nm in the particle size distribution curve of the synthesized YAG powder. The first peak is consistent with the particle size observed in the FESEM image (Fig. 2(a)) and the second is attributed to the agglomerated particle size of the ultrafine YAG powder. Therefore, the particle size distribution of the synthesized powder was not uniform, which emphasizes the need for the de-agglomeration process. The de-agglomerated ultrafine YAG powder had a uniform particle size distribution with the mean particle size of 259 nm which is in a good agreement with FESEM image (Fig. 2(b)). It is deduced from DLS curves that after the de-agglomeration process, the uniform and narrow particle size distribution of the ultrafine YAG powder was obtained. However, without this process, non-uniform and broad particle size distribution would be observable.

The viscosity and shear stress of the de-agglomerated ultrafine YAG powder slurry with 55 wt% solid load versus the shear rate for different contents of the dispersant is demonstrated in Fig. 4. It shows that the rheology of suspensions depends on the amount of the dispersant agent. Slip casting without dispersant displays a slight shear thinning behavior. The breakdown of the flocculated structure and the release of the entrapped liquid are almost the reason for the slight shear thinning flow. At 0.5 to 2 wt% of dispersant, the slips are nearly Newtonian and their viscosity is constant at all shear rates indicating a well-dispersed and homogeneous slurry [6]. By further increase of the dispersant up to 2.5 wt%, a slight shear thinning was observed, implied that there is no yield point [42].

Fig. 5 shows the plot of viscosity versus the amount of dispersant for the de-agglomerated ultrafine YAG slurry with 55 wt% solid load. Up to 1.5 wt% dispersant, the viscosity was decreased, while by further increase of the dispersant agent, the viscosity of the slurry was increased. The minimum viscosity is related to the optimum amount of dispersant needed for maximum coverage of particle surface. The excess amount of dispersant
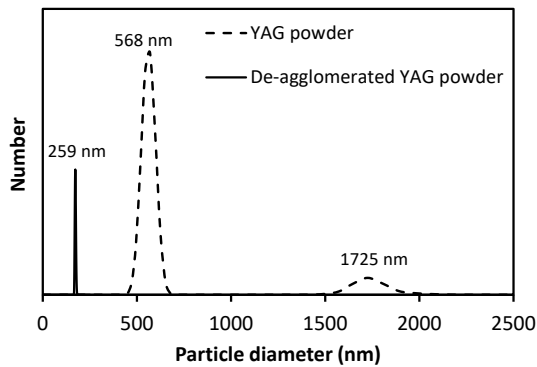
Fig. 3- Particle size distribution of the synthesized and de-agglomerated ultrafine YAG powder.
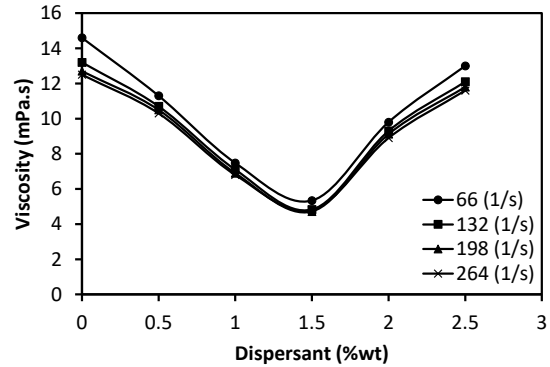
Fig.5- Viscosity vs. the amount of dispersant for de-agglomerated ultrafine YAG slurry with 55%wt solid load at different shear rates.
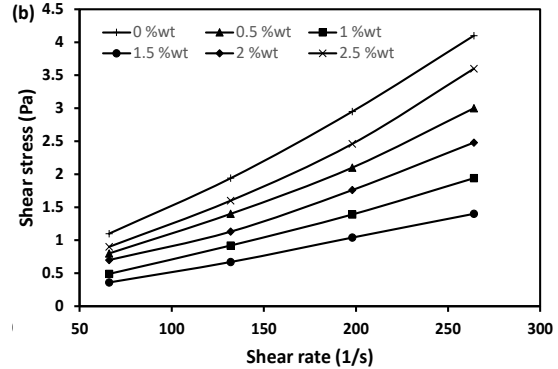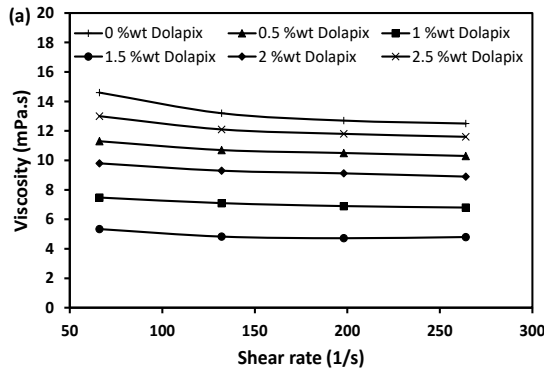
Fig. 4- (a) Viscosity vs. shear rate curves and (b) shear stress vs shear rate curves for de-agglomerated ultrafine YAG slurry with 55 wt% solid load at different contents of Dolapix dispersant.

acts as a free electrolyte and leads to depletion flocculation, whereas insufficient dispersant concentration does not result in dispersion of whole particles [7]. In both cases, the viscosity of suspension increases due to agglomerates present in the slurry [43].

The rheological behavior of the YAG slurries with 1.5 wt% Dolapix dispersant was studied by measuring the viscosity and shear stress at different shear rates (Fig. 6) which is strongly dependent on the solid loading. For instance, near-Newtonian behavior is exhibited at a solid loading lower than 55 wt%, whereas slight shear thinning behavior is observed at solid loading of 65 wt%. The rheological behavior of the slurry has been changed completely into shear thinning at 75 wt% solid loading. At high solid load, the liquid becomes immobilized in the inter-particulate pore spaces of the flocculated network of slurry. Applying shear stress breakdowns the flocculated structure and releases the entrapped liquid [12, 44]. Furthermore, Increasing the solid load leads to the mean path between particles falling down and; hence, flocculation occurs as a result of increased attraction force between

particles. Therefore, particles form either a particle network or individual clusters in the suspension which increases the viscosity value [27, 45].

The green density of slip cast bodies was in the range of 48-65% of the YAG theoretical density. It can be observed from Fig. 7 that the green density is enhancing (by about 15%) if the solid loading was increased from 55% to 75 wt%. The highest green density of 65% theoretical value was obtained at optimum 75 wt% solid load at optimum dispersant condition. By further increase of the solid loading, the green density of slip cast bodies was decreased. The highest state of flocculation in slurries with 80 wt% solid load is the reason of high viscosity which leads to reducing the green density. The formation of strong aggregates might be due to non-homogeneous distribution of dispersant molecules on particles of high solid loading slurry. Therefore, not a complete coverage of YAG particles in 80 wt% slurry with dispersant causes coagulation and reduction in particle packing efficiency which seems to have detrimental influence on the green density [46, 47]. The formation of large pores due to flocculates also causes a reduction in homogeneity and; hence, in green density of slip cast bodies [32, 48, 49].

Fig. 8 shows the pore size distribution of the slip cast green body processed by slurry with 75% solid load. One narrow pore size distribution peak located at 286 nm is obtained by the slip casting of the de-agglomerated ultrafine YAG powder. The peak achieved at almost half of the particle size of synthesized powders is an important factor in evaluating slip cast green bodies [26]. This uniform pore size distribution of the slip cast green body is related to the appropriate morphology of the de-agglomerated ultrafine YAG powder and optimized
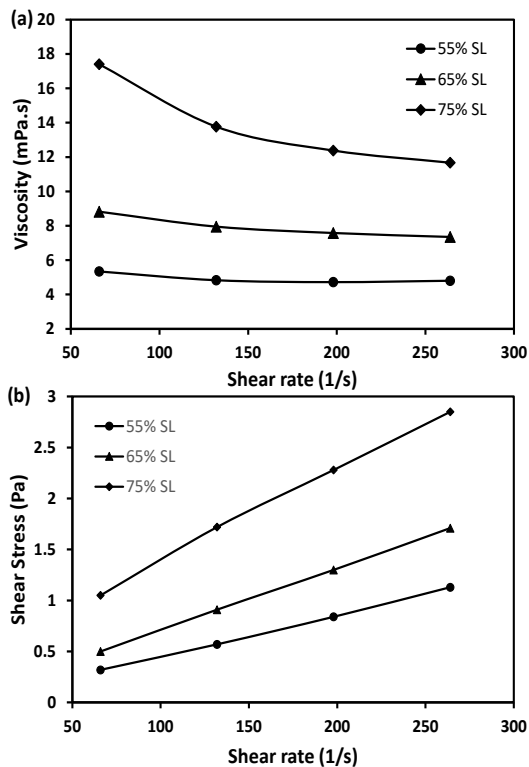
Fig. 6- Viscosity vs. shear rate curves and (b) shear stress vs. shear rate curves for de-agglomerated ultrafine YAG slurry with 1.5 %wt Dolapix as a function of solid loading.
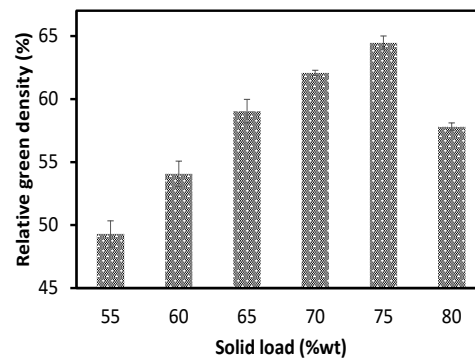
Fig. 7- Relative green density vs. solid load for slip casted samples (three or four samples for each solid load were slip casted).

slip cast parameters used for preparing the green body.

Fig. 9 shows the microstructure of the fracture surface of the green body with 75 wt% solid load and 1.5 wt% dispersant. In these conditions, a uniform microstructure can be observed. This homogeneity indicates that 1.5 wt% Dolapix is sufficient to disperse correctly the de-agglomerated ultrafine YAG powders. This result is in a good agreement with the above mentioned discussion results.

Fig. 10 compares the FESEM micrographs of slip casting fracture surfaces with different green densities sintered in the air at 1720°C for 12h. Generally, it was observed that by increasing the green density of samples, better densification occurs during sintering in the air. It can be seen that higher densification of slip cast bodies leads to the fewer and also smaller pore sizes in the sintered bodies [46]. The grain size in the sample with the lowest green density (50%, Fig. 10(a)) was about 4 μm. The results show that increasing the relative

Fig. 8- Pore size distribution of green body with 75% wt solid load.
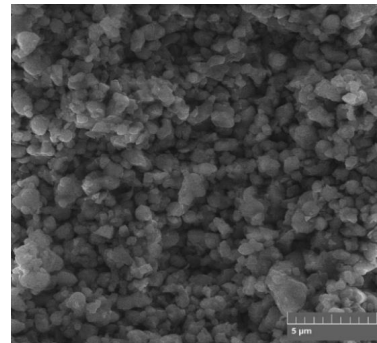
Fig. 9- FESEM micrograph of fracture surface of slip cast YAG green body with 75%wt solid load.
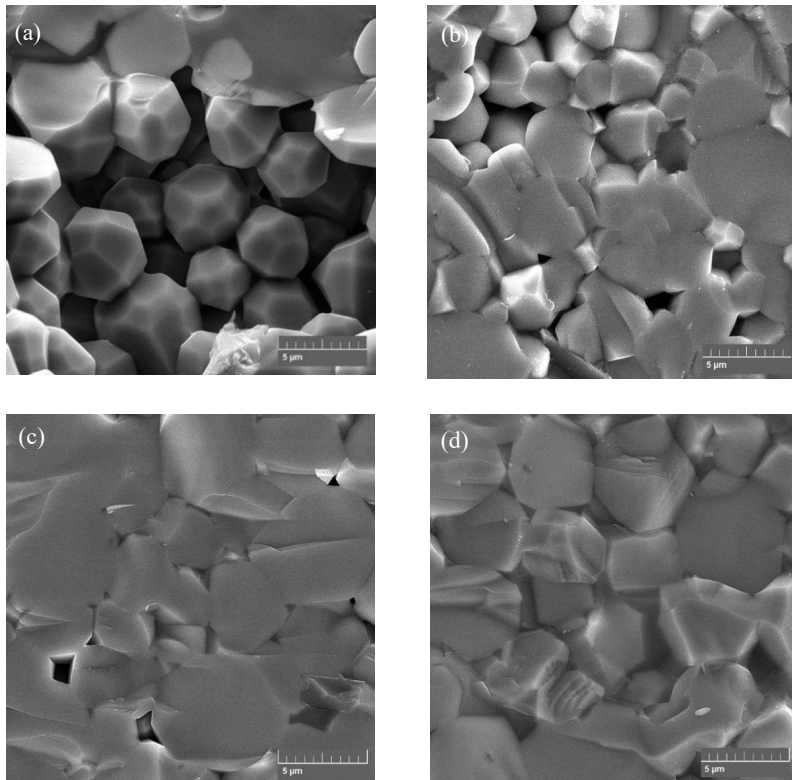
Fig. 10- FESEM micrographs of fracture surfaces of ultrafine YAG sintered bodies in the air atmosphere (1720°C for 12 h) of different slip cast samples with different relative green densities: (a) 50%, (b) 55%, (c) 60% and (d) 65%.

green density of slip cast bodies (65%, Fig. 10(d)) did not have a significant effect on the grain growth during sintering in the air atmosphere.

Fig. 11 displays the FESEM micrographs of the YAG fracture surface vacuum sintered at 1700 ˚C for 12h. From Fig. 11 (a) and (b), we can see large pores in vacuum sintered samples with 50% as well as 55% green density. By further increase of the relative green density to 60%, few pores could be captured in the lattice of grains and also grain boundaries (Fig. 11 (c)). A dense and pore-free microstructure can be observed at vacuum sintered specimen with 65% relative green density. The average grain size was about 5-7 μm (Fig. 11(d)) which was similar to that reported in the literatures [5, 9, 10]. Furthermore, the micrographs indicated that the grain size was increased and the pore size was decreased by increasing the relative green density of slip cast bodies used for vacuum sintering. Final pores removal and attaining fully dense YAG ceramic are controlled by grain growth [9]. These observations show that final stage of the YAG densification in vacuum atmosphere is

accompanied by a significant grain growth which is consistent with the results reported by Boulesteix et al. [50]. Hence, promoting grain growth at the final stage of sintering is an effective way for reducing the number of pores in YAG ceramic.

Fig. 12 shows the relative density after sintering in the air and vacuum atmospheres of various slip cast bodies with 50%, 55%, 60%, and 65% relative green densities. It can be observed that in both sintering methods, the relative density of the sample after sintering has been enhanced by increasing the green density of the slip cast body. Additionally, it is obvious that although the green densities of slip cast bodies were the same, the density of vacuum sintered bodies was higher than air atmosphere sintered bodies. These results show the capacity of vacuum sintering method for obtaining samples with high densities. Another point is that the sintered bodies with 65% relative green density have been densified to 99.9% and 98% relative density by sintering in vacuum and air atmosphere+s, respectively. Therefore, pores are
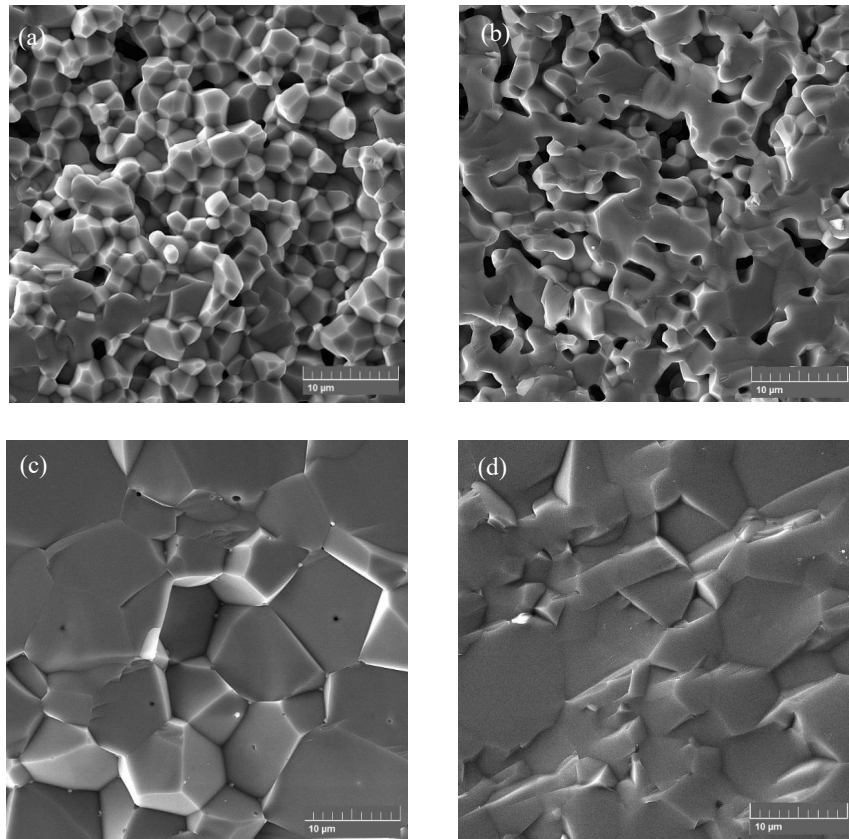
Fig. 11- FESEM micrographs of fracture surfaces of ultrafine YAG vacuum sintered bodies (1700˚C for 12 h) of different relative green densities: (a) 50%, (b) 55%, (c) 60% and (d) 65%.

effectively eliminated in vacuum sintering method by using slip cast bodies with high relative green densities. There is nearly no gas in the pores in vacuum sintering. Therefore, the elimination of pores is easy with this method of sintering. The air is composed of 79% nitrogen gas with 1.71 Å size. In spite of the fact that entrapped oxygen gas in pores can easily migrate through lattice vacancies [51], too big size of nitrogen atoms leads to the low solubility in the YAG crystal lattice and the diffusion through them is negligible compared to those of oxygen [33, 52]. High diffusion coefficient at high temperature as well as the small size of oxygen molecules let them dissolve into the YAG crystal and remove easily during the sintering process [53]. In addition, the high partial pressure of oxygen depresses the grain boundary mobility and causes more pores to be eliminated during sintering [54]. Filling the pores with inert gases such as argon or nitrogen during the final stage of sintering causes the pores to remain and then increase in size by uniting them together [51]. Trapped air in the pore balances the material transporting through making high enough pressure. Hence, the elimination of this kind of pores during the sintering is difficult and inhibits further densification. The kind of trapped gas in the pores is an important factor in densification process which is influenced by diffusion rate of the gas [51]. Therefore, nitrogen gas is the main problem in the sintering of YAG ceramic in the air and is also observed in other optical ceramics such as Y_2O_3 and Al_2O_3 [53, 55].
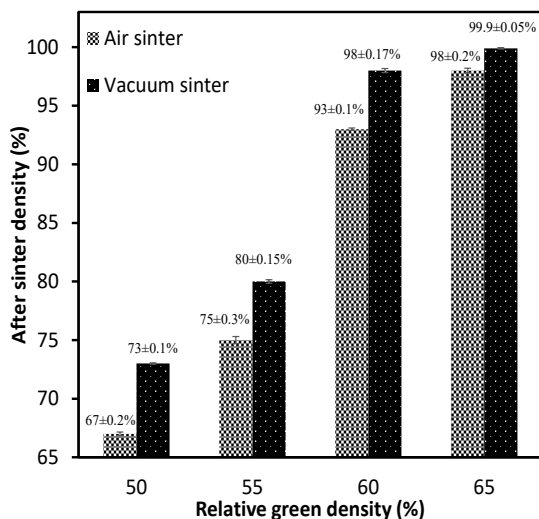
Fig. 12- The relative density of samples after sintering in air atmosphere and in vacuum atmosphere vs. relative green density of YAG slip cast green bodies.

4. Summary

It is revealed in the present study that homogeneous microstructure and high density of the YAG green body can be prepared by appropriate dispersion of the ultrafine YAG particles using the slip casting method. The best dispersion of the de-agglomerated ultrafine YAG particles was observed at 1.5 wt% Dolapix, as revealed by minimum viscosity and near-Newtonian behavior of the slurry. The slip with a solid loading of 55 wt% exhibited near-Newtonian behavior, whereas with higher solid loading of about 65 and 75 wt%, the behavior of slips changed to a slight shear thinning. At the optimum dispersant value (1.5 wt%), a 75 wt% solid loaded green body displayed mono modal pore size distribution centered at half of the synthesized ultrafine YAG powder size. The density after sintering in vacuum atmosphere was higher for all starting green densities.

References

1. Frage N, Kalabukhov S, Sverdlov N, Ezersky V, Dariel MP. Densification of transparent yttrium aluminum garnet (YAG) by SPS processing. Journal of the European Ceramic Society. 2010;30(16):3331-7.
2. Sokol M, Kalabukhov S, Kasiyan V, Rothman A, Dariel MP, Frage N. Mechanical, thermal and optical properties of the SPS-processed polycrystalline Nd:YAG. Optical Materials. 2014;38:204-10.
3. Ikesue A, Yoshida K, Yamamoto T, Yamaga I. Optical scattering centers in polycrystalline Nd: YAG laser. Journal of the American Ceramic Society. 1997;80(6):1517-22.
4. Irankhah R, Zakeri M, Rahimipoor MR, Razavi M. In-situ Fabrication of Transparent Magnesium Aluminate Spinel by Spark Plasma Sintering. Advanced Ceramics Progress. 2017;3(1):6-9.
5. Lv Y, Zhang W, Tan J, Sang Y, Qin H, Hu J, et al. Dispersion of concentrated aqueous neodymia–yttria–alumina mixture with ammonium poly(acrylic acid) as dispersant. Journal of Alloys and Compounds. 2011;509(6):3122-7.
6. Li X, Li Q. YAG ceramic processed by slip casting via aqueous slurries. Ceramics International. 2008;34(2):397-401.
7. Appiagyei KA, Messing GL, Dumm JQ. Aqueous slip casting of transparent yttrium aluminum garnet (YAG) ceramics. Ceramics International. 2008;34(5):1309-13.
8. Guo W, Cao Y, Huang Q, Li J, Huang J, Huang Z, et al. Fabrication and laser behaviors of Nd:YAG ceramic microchips. Journal of the European Ceramic Society. 2011;31(13):2241-6.
9. Ji X, Deng J, Kang B, Huang H, Wang X, Jing W, et al. Fabrication of transparent neodymium-doped yttrium aluminum garnet ceramics by high solid loading suspensions. Ceramics International. 2013;39(7):7921-6.
10. Guo W, Huang J, Lin Y, Huang Q, Fei B, Chen J, et al. A low viscosity slurry system for fabricating chromium doped yttrium aluminum garnet (Cr:YAG) transparent ceramics. Journal of the European Ceramic Society. 2015;35(14):3873-8.
11. Esposito L, Piancastelli A. Role of powder properties and shaping techniques on the formation of pore-free YAG materials. Journal of the European Ceramic Society. 2009;29(2):317-22.
12. Lv Y-H, Liu H, Sang Y-H, Liu S-J, Chen T, Qin H-M, et al.

Electrokinetic properties of Nd:YAG nanopowder and a high concentration slurry with ammonium poly(acrylic acid) as dispersant. Journal of Materials Science. 2010;45(3):706-12.

13. Ba X, Li J, Pan Y, Zeng Y, Liu W, Jiang B, et al. Influences of Solid Loadings on the Microstructures and the Optical Properties of Yb:YAG Ceramics. International Journal of Applied Ceramic Technology. 2013;12(2):418-25.

14. Mohammadi F, Mirzaee O, Tajally M. Influence of solid loading on the rheological, porosity distribution, optical and the microstructural properties of YAG transparent ceramic. Ceramics International. 2018;44(11):12098-105.

15. Mohammadi F, Mirzaee O, Tajally M. Influence of TEOS and MgO addition on slurry rheological, optical, and microstructure properties of YAG transparent ceramic. Optical Materials. 2018;85:174-82.

16. Hreniak D, Stręk W. Synthesis and optical properties of Nd3+-doped Y3Al5O12 nanoceramics. Journal of Alloys and Compounds. 2002;341(1-2):183-6.

17. Zhang X, Liu D, Sang Y, Liu H, Wang J. Effects of aging on the characteristics of Nd:YAG nano-powders. Journal of Alloys and Compounds. 2010;502(1):206-10.

18. Deineka TG, Doroshenko AG, Mateychenko PV, Tolmachev AV, Vovk EA, Vovk OM, et al. Influence of sulfate ions on properties of co-precipitated Y3Al5O12:Nd3+ nanopowders. Journal of Alloys and Compounds. 2010;508(1):200-5.

19. Chen Z-H, Yang Y, Hu Z-G, Li J-T, He S-L. Synthesis of highly sinterable YAG nanopowders by a modified co-precipitation method. Journal of Alloys and Compounds. 2007;433(1-2):328-31.

20. Zhang WX, Zhou J, Liu WB, Li J, Wang L, Jiang BX, et al. Fabrication, properties and laser performance of Ho:YAG transparent ceramic. Journal of Alloys and Compounds. 2010;506(2):745-8.

21. Wen L, Sun X, Xiu Z, Chen S, Tsai C-T. Synthesis of nanocrystalline yttria powder and fabrication of transparent YAG ceramics. Journal of the European Ceramic Society. 2004;24(9):2681-8.

22. Yang H, Zhang J, Qin X, Luo D, Ma J, Tang D, et al. Polycrystalline Ho:YAG Transparent Ceramics for Eye-Safe Solid State Laser Applications. Journal of the American Ceramic Society. 2011;95(1):52-5.

23. Yang H, Qin X, Zhang J, Ma J, Tang D, Wang S, et al. The effect of MgO and SiO2 codoping on the properties of Nd:YAG transparent ceramic. Optical Materials. 2012;34(6):940-3.

24. Liu W, Zhang W, Li J, Kou H, Shen Y, Wang L, et al. Influence of pH values on (Nd+Y):Al molar ratio of Nd:YAG nanopowders and preparation of transparent ceramics. Journal of Alloys and Compounds. 2010;503(2):525-8.

25. Ikesue A, Furusato I, Kamata K. Fabrication of Polycrystal line, Transparent YAG Ceramics by a Solid-State Reaction Method. Journal of the American Ceramic Society. 1995;78(1):225-8.

26. Krell A, Klimke J. Effects of the Homogeneity of Particle Coordination on Solid-State Sintering of Transparent Alumina. Journal of the American Ceramic Society. 2006;89(6):1985-92.

27. Lewis JA. Colloidal Processing of Ceramics. Journal of the American Ceramic Society. 2004;83(10):2341-59.

28. Evanko CR, Dzombak DA, Novak JW. Influence of surfactant addition on the stability of concentrated alumina dispersions in water. Colloids and Surfaces A: Physicochemical and Engineering Aspects. 1996;110(3):219-33.

29. Ghatee M, Salihi H. Investigation of the mechanical properties of various yttria stabilized zirconia based thin films prepared by aqueous tape casting. Advanced Ceramics Progress. 2017;3(1):26-30.

30. Krell A, Hutzler T, Klimke J, Potthoff A. Fine-Grained Transparent Spinel Windows by the Processing of Different Nanopowders. Journal of the American Ceramic Society. 2010;93(9):2656-66.

31. Tallon C, Limacher M, Franks GV. Effect of particle size on the shaping of ceramics by slip casting. Journal of the European Ceramic Society. 2010;30(14):2819-26.

32. Shafeiey A, Enayati MH, Al-Haji A. The effect of slip casting parameters on the green density of MgAl 2 O 4 spinel. Ceramics International. 2017;43(8):6069-74.

33. Tong H, Wang N, Zou Y, Zhang Z, Fan W, Shou J, et al. Densification and Mechanical Properties of YAG Ceramics Fabricated by Air Pressureless Sintering. Journal of Electronic Materials. 2018;48(1):374-85.

34. Bhattacharyya S, Mukhopadhyay TK, Dana K, Ghatak S. Pressureless reaction sintering of yttrium aluminium garnet (YAG) from powder precursor in the hydroxyhydrogel form. Ceramics International. 2011;37(8):3463-8.

35. Sang Y, Qin H, Liu H, Zhao L, Wang Y, Jiang H, et al. Partial wet route for YAG powders synthesis leading to transparent ceramic: A core–shell solid-state reaction process. Journal of the European Ceramic Society. 2013;33(13-14):2617-23.

36. Guo D, Zhao L, Sang Y, Liu H, Liu S, Sun X. Al2O3/ yttrium compound core–shell structure formation with burst nucleation: a process driven by electrostatic attraction and high surface energy. RSC Adv. 2014;4(98):55400-6.

37. Kafili G, Movahedi B, Milani M. A comparative approach to synthesis and sintering of alumina/yttria nanocomposite powders using different precipitants. Materials Chemistry and Physics. 2016;183:136-44.

38. Kafili G, Loghman-Estarki MR, Milani M, Movahedi B. The effects of TEOS on the microstructure and phase evolutions of YAG phase by formation of alumina/yttria core-shell structures. Journal of the American Ceramic Society. 2017;100(9):4305-16.

39. Guo D, Ma B, Zhao L, Qiu J, Liu W, Sang Y, et al. Bright YAG:Ce Nanorod Phosphors Prepared via a Partial Wet Chemical Route and Biolabeling Applications. ACS Applied Materials & Interfaces. 2016;8(19):11990-7.

40. Kafili G, Movahedi B, Dini G, Milani M. Yttria shell thickness estimation of alumina/yttria core/shell nanoparticles via X-ray diffraction analysis. Materials Chemistry and Physics. 2019;223:564-8.

41. Test Methods for Density of Compacted or Sintered Powder Metallurgy (PM) Products Using Archimedes Principle. ASTM International.

42. Barnes HA, Hutton JF, Walters K. An introduction to rheology: Elsevier; 1989.

43. Khan AU, Briscoe BJ, Luckham PF. Interaction of binders with dispersant stabilised alumina suspensions. Colloids and Surfaces A: Physicochemical and Engineering Aspects. 2000;161(2):243-57.

44. Ring TA. Ceramic Powder Synthesis. Fundamentals of Ceramic Powder Processing and Synthesis: Elsevier; 1996. p. 81-3.

45. Cinar S. Rheological behavior of oxide nanopowder suspensions. 2013.

46. Michálková M, Ghillányová K, Galusek D. The influence of solid loading in suspensions of a submicrometric alumina powder on green and sintered pressure filtrated samples. Ceramics International. 2010;36(1):385-90.

47. Liu D-M. Influence of solid loading and particle size distribution on the porosity development of green alumina ceramic mouldings. Ceramics International. 1997;23(6):513-20.

48. Ferreira JMF. Role of the clogging effect in the slip casting process. Journal of the European Ceramic Society.

1998;18(9):1161-9.

49. Olhero SM, Ferreira JMF. Influence of particle size distribution on rheology and particle packing of silica-based suspensions. Powder Technology. 2004;139(1):69-75.

50. Boulesteix R, Maître A, Chrétien L, Rabinovitch Y, Sallé C. Microstructural Evolution During Vacuum Sintering of Yttrium Aluminum Garnet Transparent Ceramics: Toward the Origin of Residual Porosity Affecting the Transparency. Journal of the American Ceramic Society. 2013;96(6):1724-31.

51. Choi JJ, Ryu J, Kim HE. Microstructural evolution of transparent PLZT ceramics sintered in air and oxygen atmospheres. Journal of the American Ceramic Society.

2001;84(7):1465-9.

52. Paek YK, Eun KY, Kang SJL. Effect of Sintering Atmosphere on Densification of MgO-Doped Al2O3. Journal of the American Ceramic Society. 1988;71(8):C-380-C-2.

53. Huang Y, Jiang D, Zhang J, Lin Q, Huang Z. Sintering of Transparent Yttria Ceramics in Oxygen Atmosphere. Journal of the American Ceramic Society. 2010;93(10):2964-7.

54. Chen P-L, Chen IW. Grain Boundary Mobility in Y2O3: Defect Mechanism and Dopant Effects. Journal of the American Ceramic Society. 1996;79(7):1801-9.

55. Coble RL. Sintering Alumina: Effect of Atmospheres. Journal of the American Ceramic Society. 1962;45(3):123-7.